

Obvious enhancement of the total reaction cross sections for $^{27,28}\text{P}$ with ^{28}Si target and the possible relevant mechanisms

Z.H. Liu, M. Ruan, Y.L. Zhao, H.Q. Zhang, F.

Yang, Z.Y. Ma, C.J. Lin, B.Q. Chen, Y.W. Wu

China Institute of Atomic Energy, Beijing 102413, China

W.L. Zhan, Z.Y. Guo, G.Q. Xiao, H.S. Xu, Z.Y. Sun, J.X. Li, Z.J. Chen

Institute of Modern Physics, Chinese Academy of Science, Lanzhou 730000, China

(Dated: December 23,2003)

Abstract

The reaction cross sections of $^{27,28}\text{P}$ and the corresponding isotones on Si target were measured at intermediate energies. The measured reaction cross sections of the $N = 12$ and 13 isotones show an abrupt increase at $Z = 15$. The experimental results for the isotones with $Z \leq 14$ as well as ^{28}P can be well described by the modified Glauber theory of the optical limit approach. The enhancement of the reaction cross section for ^{28}P could be explained in the modified Glauber theory with an enlarged core. Theoretical analysis with the modified Glauber theory of the optical limit and few-body approaches underpredicted the experimental data of ^{27}P . Our theoretical analysis shows that an enlarged core together with proton halo are probably the mechanism responsible for the enhancement of the cross sections for the reaction of $^{27}\text{P}+^{28}\text{Si}$.

PACS numbers: 21.10.Ft, 25.60.-t, 25.60.Dz, 27.30.+t

I. INTRODUCTION

Recently, Navin et al [1] have confirmed the important role of the $\pi s_{1/2}$ orbital in the predicted halo structure [2, 3, 4] of the neutron-deficient phosphorus isotopes $^{26,27,28}\text{P}$ by measurements of deexcitation γ ray in coincidence with the momentum distribution of the projectile residues. However, the measurements [5] of reaction cross sections for $^{27,28}\text{P}+^{12}\text{C}$ at intermediate energies do not show proton-halo structure in ^{28}P . Generally speaking, large halos are possible only for valence-neutrons in the s- and p-states, and the effect of the Coulomb barrier would hinder the formation of a proton halo [6]. Hence, proton halos are more difficult to probe experimentally, and the conclusions extracted may be not clear cut. ^8B is a typical example. Many experiments [7, 8, 9, 10] have been devoted to studies of ^8B in order to establish its halo nature. Although investigated in considerable details, its halo character has been in controversy till recent years. Similar situation may occur in ^{28}P . Thus, it is an interesting problem whether the proton halo structure really exists in ^{28}P or how large the halo is if existed. Moreover, recent studies of nitrogen, oxygen, fluorine isotopes show an abrupt rise in interaction cross section (σ_I) at $N=15$ [11] which are underpredicted even with 100% s-wave probability of a valence neutron in a “core-plus-neutron” halo model [11, 12]. It is proposed that a core modification takes place in these nuclei [12]. Kanungo et al [13] measured the longitudinal momentum distributions of one- and two-neutron removal fragments ($^{21,22}\text{O}$) of ^{23}O from the reaction with a carbon target at 72 MeV/nucleon. Their results indicate the modification of core (^{22}O) structure for the sd shell nuclei near the neutron-drip line. The present work is motivated by the observations of this new type of an anomaly in sd shell nuclei. For this purpose, reaction cross sections of isotonic nuclei with $N=12$ and 13 on Si target were measured, and special attentions were paid to the nuclei with $Z=15$, i.e., $^{27,28}\text{P}$.

II. EXPERIMENTAL PROCEDURE AND RESULTS

The experiment was performed at the Institute of Modern Physics, Lanzhou. Secondary beams of $^{27,28}\text{P}$ and the corresponding isotones were produced by the projectile fragmentation of an ^{36}Ar primary beam on a Be production target at 69 MeV/nucleon. The Be production target was 98.8 mg/cm² in thickness. The isotopes of the secondary beams were separated and selected by the magnetic rigidity of Radioactive Ion Beam Line in Lanzhou (RIBLL) [5] which served as a double-achromatic magnetic spectrometer in the present experiment. An Al energy degrader was used to improve the momentum resolution and purity

of the secondary beams. The time of flight (TOF) of the projectiles was determined by two scintillators placed at the first and second achromatic focal planes of RIBLL 16.8 m apart. The resolution of TOF was 4 ns. The position information was given by two parallel-plate-avalanche counters (PPACs) placed in the front of and behind the second scintillator. Finally, a telescope consisting of seven transmission Si surface barrier detectors was installed after the second PPAC. The thicknesses of these detectors were 150 μm for the first one and 300 μm for the others. The TOF information along with the energy deposition (ΔE_i) in the Si detectors were used to identify those projectiles of interest which underwent reactions. Fig. 1 illustrates a typical two-dimensional plot of TOF versus ΔE_2 . It is seen from the figure that particles can be identified clearly by using TOF and ΔE_i . Apart from ΔE detection, some of the Si detectors also served as the reaction target. Hence, the use of multiple Si detectors permits simultaneous measurement of reaction cross sections (σ_R) for several different energies.

Our data analysis procedure is similar to that used by Warner et al [14, 15]. A tight gate on PPACs, TOF and ΔE_i was set for each detector to identify projectiles which had not yet reacted in that and preceding detectors. Fig. 2 shows a spectrum of the total energy deposited in the telescope by ^{28}P projectiles. Events left the dotted line were counted as reaction ones. The probability η_1 for a reaction to occur beyond the first Si detector was determined by the ratio of the reaction events to the total events in the spectrum which was gated on PPACs, TOF and ΔE_1 . Likewise, the probability η_{i+1} for a reaction to take place beyond the $(i + 1)$ st detector was found from a total energy spectrum gated on PPACs, TOF and ΔE s of the $(i + 1)$ st and all preceding Si detectors. From the measured η_i and η_{i+1} , the average σ_R corresponding to the reactions taken place in the i th Si detector was determined by

$$\sigma_R = \frac{A}{\nu\rho(\Delta x)_i} \ln \left[\frac{1 - \eta_{i+1}}{1 - \eta_i} \right], \quad (1)$$

here A and ρ are atomic mass number and density of target, ν is Avogadro's number, and $(\Delta x)_i$ the thickness of ΔE_i . The σ_R was corrected for the reaction events under the elastic peak by extrapolating the spectrum left the dotted line. This correction only accounts for a few percentages of the total reaction cross section. The error in σ_R includes the statistics, uncertainties of the detector thickness and the extrapolation of reaction events. The measured reaction cross sections are listed in Table 1.

Fig.3 shows the measured σ_R (solid squares) as a function of Z for isotones with N=12 and 13 at 40 MeV/nucleon. It is worth to note that σ_R increases obviously at Z=15. The situation is very similar to the nitrogen, oxygen, fluorine isotopes where a large increase in σ_I at N=15 was observed [11, 12]. This similarity may be a signature of charge-independence of nuclear force in the nuclei far from β -stability line. In addition, it is seen that the rise of cross section for ^{27}P (even N case) is much more abrupt than that for ^{28}P (odd N case). Again, this feature is very similar to the nitrogen, oxygen, fluorine isotopes [12]. In the latter case, for the even Z nuclei (^{11}Be , ^{19}C , ^{23}O) the rise of cross section is rather abrupt, however for the odd Z nuclei (^{22}N , ^{24}F) the cross section shows a continuously increasing trend. These even-odd features are probably a reflection of the effect of pairing interaction [12].

III. MODIFIED GLAUBER MODEL ANALYSIS

A halo nucleus is considered to be composed of a core with one or two loosely bound nucleons tunneling out at distances far away from the core [16]. An abrupt enhancement of cross section of a nucleus compared to its preceding isotope/isotone neighbours can be a signature of a halo structure. The structure of halos is usually analyzed by the "core-plus-halo nucleon(s)" model [12, 13], which is realized with a few-body (FB) Glauber model [17, 18]. In the FB Glauber model, the projectile is decomposed into a core and halo nucleons, and the spatial correlation between core, halo nucleons and target are explicitly taken into account [17, 18, 19]. When the nucleus has only one halo nucleon, the reaction cross section is given by,

$$\sigma_R^{FB} = \int d\mathbf{b} \{1 - |\langle \varphi_0 | \exp [i\chi_{FT}(\bar{\mathbf{a}}) + i\chi_{nT}(\bar{\mathbf{a}} + \mathbf{s}_1)] | \varphi_0 \rangle|^2\}, \quad (2)$$

$$i\chi_{FT}(\bar{\mathbf{a}}) = - \int ds T_F(\mathbf{s}) \int dt T_T(\mathbf{t}) \Gamma(\bar{\mathbf{a}} + \mathbf{s} - \mathbf{t}), \quad (3)$$

$$i\chi_{nT}(\bar{\mathbf{a}} + \mathbf{s}_1) = - \int dt T_T(\mathbf{t}) \Gamma(\bar{\mathbf{a}} + \mathbf{s}_1 - \mathbf{t}), \quad (4)$$

where \mathbf{b} is a two dimension vector of the impact parameter which is perpendicular to the incident direction, $\bar{\mathbf{a}} = \mathbf{b} - \frac{1}{A}\mathbf{s}_1$ is the impact parameter vector of core, A is the mass number of the projectile, \mathbf{s}_1 is the perpendicular component of the halo nucleon coordinate with respect to the mass center of the core, and φ_0 is the bound state wave function. χ_{FT} ,

χ_{nT} are the optical phase-shift functions of the core and halo nucleon scattering with the target, respectively. T_F is the thickness function of the core. Γ is the profile function of a nucleon-nucleon ($N - N$) scattering. In our calculations, it takes the following expression [20],

$$\Gamma(\mathbf{b}) = \frac{\sigma_{NN}}{2\pi\beta^2} (1 - i\alpha_{NN}) \exp\left(-\frac{b^2}{\beta^2}\right), \quad (5)$$

where σ_{NN} is the total $N - N$ scattering cross section, α_{NN} is the ratio of the real to the imaginary part of the forward $N - N$ scattering amplitude, and β represents for the finite range of the $N - N$ interaction, respectively. It is important to take the finite range of the $N - N$ interaction into account in order to reproduce the experimental data at low and intermediate energies [21]. The range of the $N - N$ interaction is fixed as $\beta = 1.0$ fm in the present work. The large enhancement of the experimental reaction cross sections of $^{27,28}\text{P}$ calls for careful analysis with the Glauber theory of OL and FB approaches described above.

In Fig.3, the predictions of the modified Glauber theory in the optical limit (OL) approach[21, 22] are compared with the experimental cross sections. In this approach, the Coulomb and finite range corrections are taken into account. It is verified [21, 22] that with this modified version the Glauber theory can be extended to low energy region. In our calculations, the nuclear density distributions are evaluated in a Woods-Saxon (WS) potential. The radius and diffuseness parameters are taken as $r_0 = 1.17$ fm and $a = 0.65$ fm. The depth of the WS potential is adjusted by reproducing the single proton separation energy. The proton separation energies for these isotones are also listed in Table 1. There is only one exception of ^{25}Al . Small separation energy of the valence proton in ^{25}Al results in too diffused density. To reproduce the experimental data, the neutron separation energy is used to adjust the WS potential depth in the calculation for ^{25}Al . It may be seen from Fig.3 that there is satisfactory agreement between theory and experiment for the isotones with $Z \leq 14$. The experimental datum for ^{27}P appears to be obviously greater than the calculated value. Although the reaction cross section of ^{28}P displays an enhancement in comparison with the neighbor isotone, the modified Glauber theory with a diffused density distribution of ^{28}P could describe the experimental datum.

As shown in Fig.4 the measured σ_R of $^{27}\text{Si}+^{27}\text{Si}$ can be well described by the modified Glauber theory of OL approach. In the calculations, the geometry parameters of the WS potential are fixed at the values of $r_0 = 1.17$ fm and $a = 0.65$ fm, and the depths of the

WS potential are adjusted by reproducing the valence proton separation energies of ^{27}Si and ^{28}P , respectively. Due to the depths of the WS potential are different, the root-mean-square (rms) radii of the bare and core nuclei ^{27}Si do not have the same values. The calculated rms radii are 2.854 fm and 2.997 fm for the bare and core nuclei ^{27}Si , respectively. This means that the size of the core ^{27}Si in the nucleus ^{28}P is enlarged by about 0.143 fm as compared to that of the bare nucleus ^{27}Si . Due to the Coulomb barrier the rms radius of the proton in the $2s_{1/2}$ state of ^{28}P is only $\langle r_h^2 \rangle^{1/2} = 4.016$ fm in the WS geometry $(r_0, a) = (1.17, 0.65)$ fm. Therefore, the enhancement of the measured σ_R of $^{28}\text{P}+^{28}\text{Si}$ could be described satisfactorily by the size enlargement of the core ^{27}Si and the wave function of the valence proton at $2s_{1/2}$ state in the modified Glauber theory of the OL approach. It should be pointed out that the theoretical result underestimates the reaction cross section of ^{28}P when the density distribution of ^{28}P is calculated in the nonlinear relativistic mean field theory (RMF), where the density distribution of the valence proton at $2s_{1/2}$ state is less diffused.

The nucleus ^{26}Si is an isotope with two neutron deficit. As shown in Fig.5, the Glauber theory of the OL approach gives a well description of the ^{26}Si experimental data if a diffused density distribution with the WS geometry of $(r_0, a) = (1.27, 0.9)$ fm is used. The obtained rms radius of the bare nucleus ^{26}Si is 3.190 fm. Adding one proton in the $2s_{1/2}$ state and adjusting the depth of the WS potential to fit the separation energy $S_p = 0.900$ MeV of the valence proton, with the same geometry parameters the density distributions of the core ^{26}Si and valence proton are calculated. In terms of these density distributions, the cross sections for the reaction of $^{27}\text{P}+^{28}\text{Si}$ are evaluated in the Glauber theory of the OL and FB approaches, respectively. In this calculation, the valence proton at $2s_{1/2}$ state has a relative diffused density distribution due to its weak binding energy, and therefore the core is enlarged. The rms radii of the core and valence proton extracted from these density distributions are $\langle r_c^2 \rangle^{1/2} = 3.470$ fm and $\langle r_h^2 \rangle^{1/2} = 4.875$ fm, respectively. The difference between the rms radii of the core and bare nuclei ^{26}Si is 0.280 fm. Even though the results still underpredict the experimental data, which are shown in Fig.5 as open diamonds and squares, respectively. In order to improve the agreement, we increase the WS potential diffuseness of the valence proton to $a = 1.1$ fm, meanwhile keep the radius parameter and the core density distribution fixed. In this way, the reaction cross sections of $^{27}\text{P}+^{28}\text{Si}$ are recalculated with the Glauber model of the OL and FB approaches. The resulting reaction

cross sections are increased slightly, and are still lower than the experimental data. In this case, the rms radius of the valence proton is $< r_h^2 >^{1/2} = 5.235$ fm. On the other side, the failure to reproduce the ^{27}P data in detail may reflect deficiencies in our treatment of the reaction cross section. For example, the role of Coulomb-induced reaction is not taken into account in the present modified Glauber model. However, in the cases of ^{28}P and the isotones with $Z \leq 14$ the modified Glauber theory could well describe the experimental cross sections. Therefore, the contribution of the Coulomb-induced reactions to the total reaction cross section, if any, may be not important for the system of $^{27}\text{P}+^{28}\text{Si}$ as well.

^{27}Mg and ^{28}Al are the mirror nuclei of $^{27,28}\text{P}$, respectively. Because of isospin symmetry, the level structures within each pair should be similar. Therefore, it would be very interesting to make a comparison between the mirror nuclei. Listed in Table 2 are the interaction cross section (σ_I) for $^{27}\text{Mg}+^{12}\text{C}$ [23] and reaction cross section for $^{28}\text{Al}+^{12}\text{C}$ [24] along with the results of Glauber model analysis. In these calculations, the nuclear density distributions are evaluated in the RMF theory [25, 26, 27] with the parameter NL3 [28]. We calculate the cross sections by the Glauber theory of the OL approach with and without finite range correction. It can be seen from Table 2 that the results of these calculations are in good agreement with the experimental data for ^{27}Mg , ^{28}Al , but not for $^{27,28}\text{P}$. In the case of ^{27}P , the usual Glauber theory, i.e., the theory without finite range correction, underpredicts the experimental datum about 50%. Therefore, the comparison with the mirror nuclei supplies us a collateral evidence that the proton-rich phosphorus isotopes $^{27,28}\text{P}$ should have anomalous structures.

IV. SUMMARY

The reaction cross sections of $^{27,28}\text{P}$ and the corresponding isotones on Si target are measured at intermediate energies. The measured reaction cross sections of the $N = 12$ and 13 isotones show a large increase at $Z = 15$. The experimental results for the isotones with $Z \leq 14$ as well as ^{28}P can be well described by the modified Glauber theory of the OL approach. The enhancement of the cross section for the $^{28}\text{P}+^{28}\text{Si}$ reaction could be well explained by the modified Glauber theory of the OL approach with an enlarged core. The valence proton in ^{28}P at $2s_{1/2}$ state has less diffused density distribution than usually observed in a halo nucleon. The modified Glauber theory of the OL and FB approaches somehow underpredicts the experimental data of ^{27}P . In these calculations 100% occupancy

of the valence-proton in the s-orbital is assumed. Since s-wave contribution gives the largest cross section, the results of the modified Glauber model calculation represent the up-limit predictions of “core-plus-halo nucleon(s)” model. In addition, as shown in Table 2 the modified Glauber model with the RMF theory densities also underpredict the cross section for ^{27}P . Although a satisfactory agreement between the theoretical predictions and experimental data is not reached, our theoretical analysis indicates that an enlarged core together with proton halo are probably the mechanisms responsible for the anomalous enhancement of the cross sections for the reaction of $^{27}\text{P}+^{28}\text{Si}$. However, this suggestion should be viewed as a primary theoretical explanation. Actually, the halo structure of *sd* shell proton-rich nuclei is not quite clearly understood theoretically yet. In order to prove the possible relevant mechanisms, further investigations with more sophisticated experiments and theories are required.

Acknowledgments

This work was supported by the National Natural Science Foundation of China under Grants No. 10075080, 10175092, 10235030, 10275092, 10275094 and the Major State Basic Research Development Programme under Grant No. G200007400.

-
- [1] A. Navin *et al.*, Phys. Rev. Lett. **81**, 5089 (1998).
 - [2] B.A. Brown and P.G. Hansen, Phys. Lett. B **381**, 391 (1996).
 - [3] Z.Z. Ren, B.Q. Chen, Z.Y. Ma, G.O. Xu, Phys. Rev. C **53**, 572 (1996).
 - [4] B. Q. Chen, Z. Y. Ma, F.Grümmer and S. Krewald, J. of Phys.G: Nucl. and part. Phys. **24**, 97 (1998).
 - [5] H.Y. Zhang *et al.*, Nucl. Phys. **A707**, 303 (2002).
 - [6] K. Riisager, A.S. Jensen and P. Moller, Nucl. Phys. **A548** (1992) 393.
 - [7] T. Minamisono *et al.*, Phys. Rev. Lett. **69**, 2058 (1992).
 - [8] B. Blank *et al.*, Nucl. Phys. **A624**, 242 (1997).
 - [9] F. Negoita *et al.*, Phys. Rev. C **54**, 1787 (1996).
 - [10] J.H. Kelley *et al.*, Phys. Pev. Lett. **77**, 5020 (1996).

- [11] A. Ozawa *et al.*, Nucl. Phys. **A691**, 599 (2001).
- [12] R. Kanungo, I. Tanihata, and A. Ozawa, Phys. Lett. B **512**, 261 (2001).
- [13] R. Kanungo *et al.*, Phys. Rev. Lett. **88**, 142502 (2002).
- [14] R.E. Warner *et al.*, Phys. Rev. C **52**, R1166 (1995).
- [15] R.E. Warner *et al.*, Nucl. Phys. **A635**, 292 (1998).
- [16] A.S. Jensen, K. Riisager, Phys. Lett. B **480**, 39 (2000).
- [17] Y. Ogawa, K. Yabana, and Y. Suzuki, Nucl. Phys. **A543**, 723 (1992).
- [18] J.S. Al-Khalili, J.A. Tostevin, Phys. Rev. Lett. **76**, 3903 (1996).
- [19] Y.L. Zhao, Z.Y. Ma, B.Q. Chen and W.Q. Shen, Chin. Phys. Lett. **20**, 53 (2003).
- [20] S.K. Charagi and S.K. Gupta, Phys. Rev. C **56**, 1171 (1997).
- [21] Y.L. Zhao, Z.Y. Ma, B.Q. Chen, Commun. Theor. Phys. **36**, 313 (2001).
- [22] Y.L. Zhao, Z.Y. Ma, B.Q. Chen, and X.Q. Sun, High Energy Phys. & Nucl. Phys. **25**, 506 (2001).
- [23] T. Suzuki *et al.*, Nucl. Phys. **A630**, 661 (1998).
- [24] X.Z. Cai *et al.*, Phys. Rev. C **65**, 024610 (2002).
- [25] C.J. Horowitz and B.D. Serot, Nucl. Phys. **A368**, 503 (1981).
- [26] P.G. Reinhard, M. Rufa, J. Maruhn, W. Greiner, and J. Friedrich, Z. Phys. A **323**, 13 (1986).
- [27] S.K. Para, Nucl. Phys. **A559**, 173 (1993).
- [28] G.A. Lalazissis, J. König and P. Ring, *Phys. Rev. C* **55**, 540 (1997).

TABLE I: The valence-proton separation energy, energy of projectiles, experimental reaction cross sections and theoretical reaction cross sections calculated with the Glauber model of the OL approach for the isotones with N=12 and 13. For ^{25}Al instead of proton separation energy, the neutron energy is given.

| Nucleus | S_p | E_{in} | E_{av} | E_{out} | σ_R^{exp} | σ_R^{OL} |
|------------------|---------|---------------|---------------|---------------|-------------------------|-----------------|
| | (MeV) | (MeV/nucleon) | (MeV/nucleon) | (MeV/nucleon) | (mb) | (mb) |
| ^{23}Na | 8.794 | 19.3 | 14.5 | 9.7 | 1880±150 | - |
| | | 22.7 | 22.7 | 19.3 | 2018±150 | 2010 |
| ^{24}Mg | 11.693 | 22.4 | 17.7 | 13.1 | 1993±80 | - |
| | | 29.4 | 25.9 | 22.4 | 1998±80 | 1963 |
| ^{25}Mg | 12.064 | 27.4 | 23.9 | 20.3 | 2237±133 | - |
| | | 33.4 | 30.4 | 27.4 | 2026±121 | 1967 |
| ^{25}Al | 16.932* | 25.3 | 20.6 | 15.9 | 2141±120 | - |
| | | 32.5 | 28.9 | 25.3 | 2027±110 | 1972 |
| ^{26}Al | 6.307 | 30.4 | 26.7 | 23.0 | 2164±90 | - |
| | | 36.6 | 33.5 | 30.4 | 2026±100 | 2075 |
| ^{26}Si | 5.518 | 27.9 | 23.1 | 18.4 | 2351±190 | - |
| | | 35.4 | 31.7 | 27.9 | 2284±190 | 2092 |
| ^{27}Si | 7.463 | 33.0 | 29.2 | 25.3 | 2145±80 | - |
| | | 39.5 | 36.3 | 33.0 | 2008±100 | 2050 |
| ^{27}P | 0.900 | 30.6 | 25.8 | 20.9 | 3029±380 | - |
| | | 38.4 | 34.5 | 30.6 | 2900±370 | 2302 |
| ^{28}P | 2.066 | 35.6 | 31.6 | 27.6 | 2377±110 | - |
| | | 42.4 | 39.0 | 35.6 | 2237±80 | 2210 |

TABLE II: A comparison between the mirror nuclei ^{27}Mg , ^{27}P , and ^{28}Al , ^{28}P . The neutron separation energies for ^{27}Mg and ^{28}Al , and proton separation energies for $^{27,28}\text{P}$ are given in the Table. Listed in the sixth and seventh columns are the calculated results of the Glauber model in the OL approach without and with finite range correction, respectively, where the corresponding density distributions are calculated in the RMF with the parameter set NL3.

| Nucleus | S_p (MeV) | reaction | E_{Lab} (MeV/nucleon) | σ^{exp} (mb) | $(\sigma_R^{OL})_{\text{nfc}}$ (mb) | $(\sigma_R^{OL})_{\text{fc}}$ (mb) |
|------------------|----------------|--------------------------------|----------------------------|-------------------------------|--|---------------------------------------|
| ^{27}Mg | 6.443 | $^{27}\text{Mg}+^{12}\text{C}$ | 950 | 1203 ± 16 | 1314 | 1340 |
| ^{28}Al | 7.725 | $^{28}\text{Al}+^{12}\text{C}$ | 19 | 1866 ± 121 | 1732 | 1898 |
| ^{27}P | 0.900 | $^{27}\text{P}+^{28}\text{Si}$ | 34.5 | 2900 ± 370 | 1972 | 2145 |
| ^{28}P | 2.066 | $^{28}\text{P}+^{28}\text{Si}$ | 39.0 | 2237 ± 80 | 1934 | 2109 |

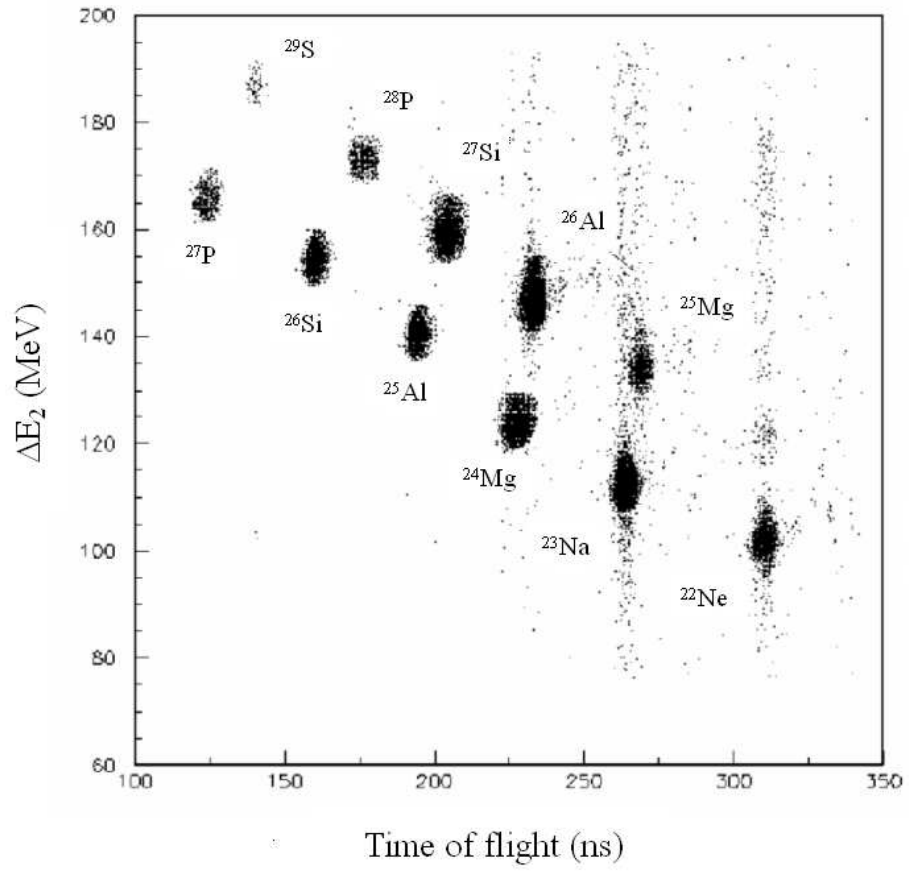


FIG. 1: Two-dimensional plot of TOF versus ΔE_2 .

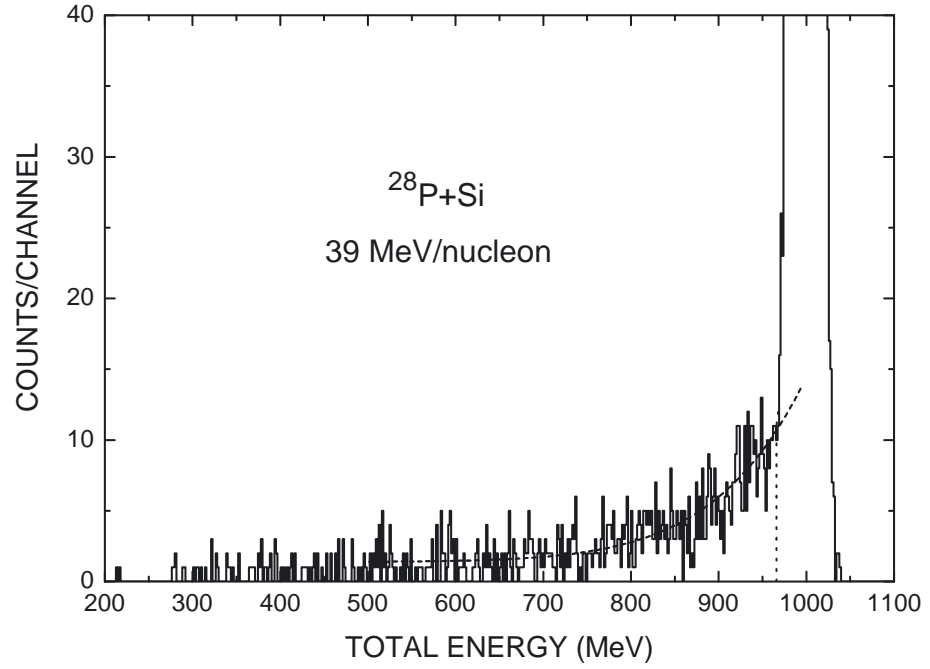


FIG. 2: Total energy deposition spectrum of ^{28}P projectile in Si telescope. Events to the left of the dotted vertical line are counted as reactions.

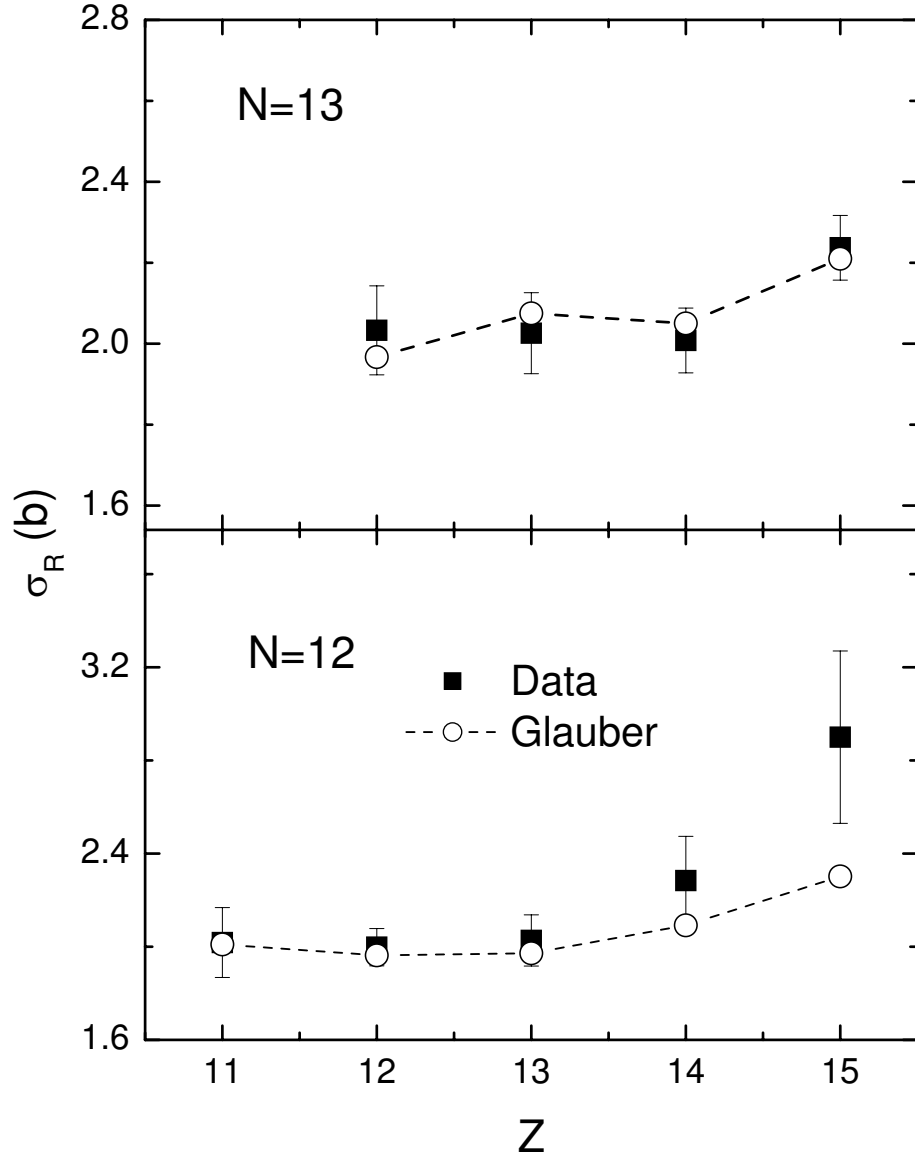


FIG. 3: The Z dependence of the reaction cross sections for the isotones with N=12 and 13 at 40 MeV/nucleon. The solid squares with error bar represent the experimental data. The open circles illustrate the prediction of the modified Glauber model in the OL approach. The symbols are connected by lines for each isotonic number to guide the eye.

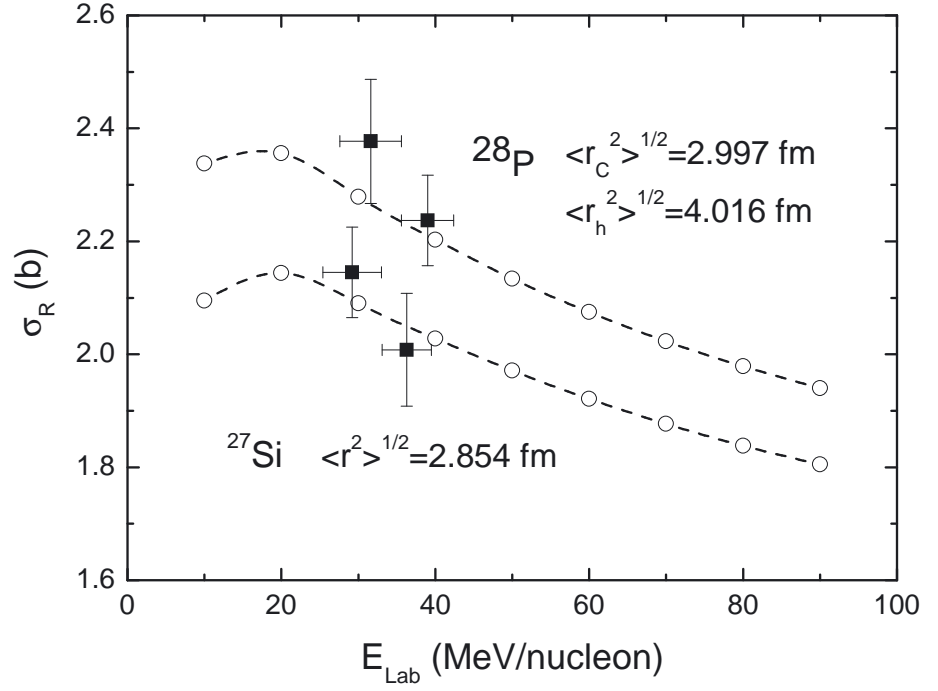


FIG. 4: Measured σ_R vs energy for the ^{27}Si , $^{28}\text{P}+^{28}\text{Si}$ reactions. The predictions of the modified Glauber model of the OL approach (open circles) are compared with the experimental data.

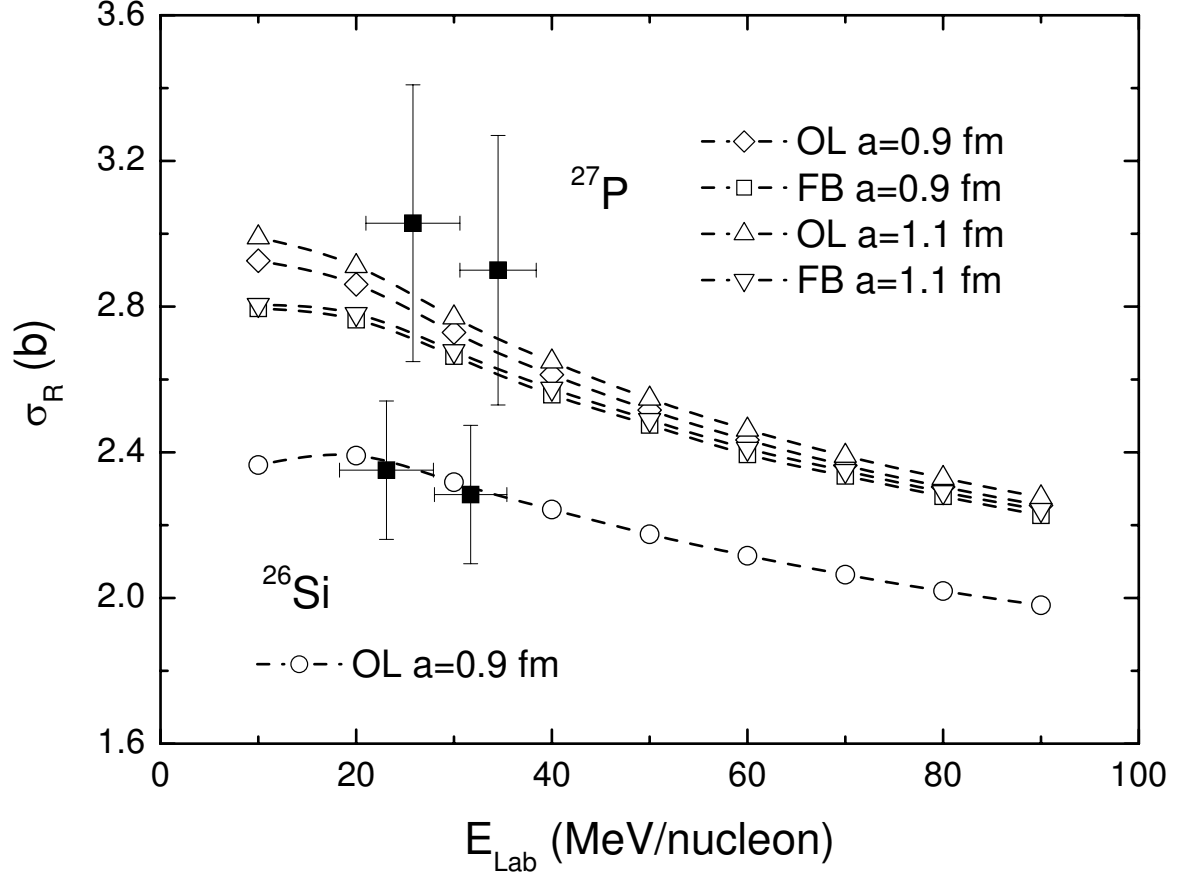


FIG. 5: Measured σ_R vs energy for the ^{26}Si , $^{27}\text{P} + ^{28}\text{Si}$ reactions. The predictions of the modified Glauber model of OL and FB approaches (open symbols) are compared with the experimental data. The numbers in the figure represent the diffuseness parameter of the WS potential for the valence proton.